Microbuckle initiation in fibre composites under multiaxial loading

By J. Y. Shu† and N. A. Fleck

Department of Engineering, University of Cambridge, Trumpington Street, Cambridge CB2 1PZ, UK

The microbuckling strength of long fibre–polymer matrix composites under multiaxial in-plane loading is analysed using a finite element code. Cosserat couple stress theory is used to include the role of fibre bending resistance, with the fibre diameter setting the internal length scale of the constitutive law. The matrix is treated as a dilatant nonlinear elastic–plastic solid. Microbuckling is assumed to nucleate from an elliptical region of initial fibre waviness. Both in-plane shear stress and transverse stress significantly knock-down the axial compressive strength. The compressive strength is found to be sensitive to both the magnitude of the fibre waviness and to the physical size of the region of waviness in relation to the fibre diameter d. The dominant geometrical feature is the length ℓ of the initial imperfection in the transverse direction: the collapse strength exceeds the infinite band prediction by less than 20% when ℓ exceeds about 200 fibre diameters.

1. Introduction

Fibre microbuckling is often the dominant compressive failure mechanism in long-fibre polymer matrix composites; it occurs by the cooperative buckling of fibres within a band and results in compressive strengths of only about $\frac{2}{3}$ of the tensile strength. There is now a substantial body of experimental and theoretical evidence to show that microbuckling is an imperfection-sensitive plastic buckling event, with the imperfection usually in the form of pre-existing fibre waviness (Argon 1972; Budiansky 1983; Budiansky & Fleck 1993). Early theories of microbuckling such as that of Rosen (1965) assumed that compressive failure is by elastic bifurcation and occurs at a strength σ_c equal to the in-plane shear modulus of the composite, G. This analysis over-predicts the compressive strength by a factor of about four. It is unfortunate that much of the previous and current literature ignores this fact and erroneously treats microbuckling as a linear elastic bifurcation event.

To date, most theoretical treatments of microbuckling are one-dimensional infinite band localization analyses and fit approximately within the framework laid down by Rice (1976) (see, for example, Slaughter *et al.* 1993; Budiansky & Fleck 1994). Collapse is assumed to initiate from an imperfection in the form of a pre-existing band of uniform fibre misalignment. Such infinite band kinking analyses neglect fibre bending resistance and suffer from two main limitations: (i) they are unable to

† Present address: Lawrence Livermore National Laboratory, L-370, Livermore, CA 94550, USA.

Proc. R. Soc. Lond. A (1997) **453**, 2063–2083
Printed in Great Britain

TEX Paper

account for the effect of the shape of the region of initial fibre misalignment upon the compressive strength; and (ii) they provide no information on the effect of the physical size of the imperfection upon the compressive strength since the assumed constitutive law contains no length scale.

Fleck *et al.* (1995) overcame the second limitation by including the effects of fibre bending resistance, with the fibre diameter d setting the material length scale. Fleck & Shu (1995) overcame both limitations by developing a two-dimensional, finite strain, finite element code for fibre microbuckling. In their analysis the composite is treated as a 'smeared-out' anisotropic nonlinear continuum with an in-plane shear and transverse response given by that of a flow-theory elastic–plastic solid. The axial behaviour is taken to be linear elastic. Cosserat couple stress theory is used to include the effects of fibre bending resistance; the fibre diameter d dictates the bending resistance and serves as the dominant length scale of the microstructure. In the finite element formulation, the nodal degrees of freedom are two in-plane displacements and the rotation of the fibre cross-section θ_f. Fleck & Shu (1995) performed a preliminary study of the effect of imperfection size and shape upon the uniaxial compressive strength. They considered an elliptical region of fibre waviness; the elliptical region was assumed to have a width w of $20d$ along the fibre direction and a length ℓ in the transverse direction in the range $\ell/d = 0$ to ∞. The fibre misalignment angle $\bar{\phi}$ was assumed to increase smoothly from zero at the edge of the elliptical imperfection to a maximum value of about 2° at the centre of the ellipse. They found that the compressive strength σ_c decreases with increasing ℓ/d from Rosen's elastic bifurcation value $\sigma_c = G$ at $\ell/d = 0$ to the infinite band compressive strength of about $\frac{1}{4}G$ at large ℓ/d. The strength is midway between the two asymptotes at $\ell/d \approx 20$.

In the present paper we build upon the previous study of Fleck & Shu (1995) and address the following three questions.

(1) *For the case of an infinite band of initial waviness, what is the knock-down factor in collapse strength due to in-plane shear loading and in-plane transverse loading?*

Slaughter *et al.* (1993) previously examined the effects of in-plane shear and transverse tensile stresses on the compressive strength by employing a kinking analysis: the fibres were taken as inextensible with vanishing bending resistance and were allowed to rotate uniformly within the kink band. The accuracy of these assumptions is now ascertained by carrying out more detailed couple stress calculations to account for the effects of fibre bending and fibre extension.

(2) *What is the sensitivity of the infinite band compressive strength to the nature of the constitutive law assumed for the composite?*

The previous finite element analysis of Fleck & Shu (1995) assumed that the in-plane response of the composite is given by a flow theory version of plasticity. Fleck & Jelf (1995) suggest that a deformation theory version of plasticity is more appropriate and such a formulation is outlined below. Here, the infinite band compressive strength is calculated for both deformation and flow theory versions of plasticity.

(3) *How does the compressive strength depend upon the shape and size of the initial region of waviness, for the case of general in-plane remote loading?*

Fleck & Shu (1995) showed that the infinite band microbuckle response is a reasonably good approximation to the collapse response from a finite region of fibre waviness under uniaxial compression along the fibre direction, provided the transverse length of the microbuckle exceeds about $200d$. Here, we examine the accuracy of the infinite band calculation for predicting the compressive strength under multiaxial loading; specifically, we determine the significance of imperfection size and

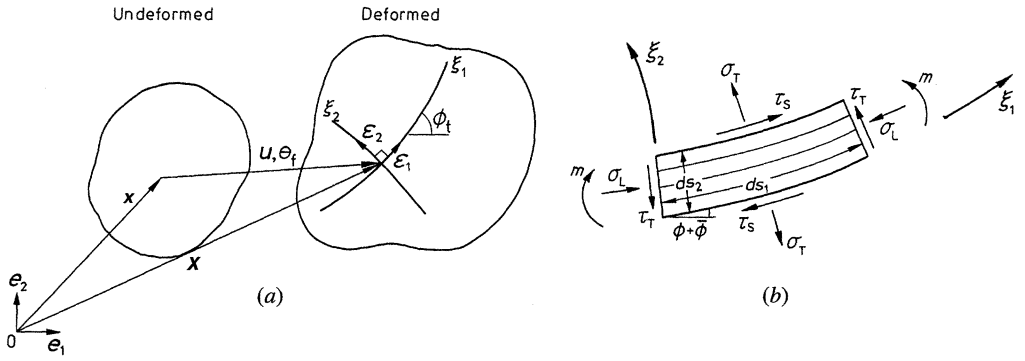

Figure 1. (*a*) Definition of coordinates and base vectors. (*b*) Stress state of a representative volume element of the fibre composite.

shape upon the collapse strength under general in-plane loading. The effect of fibre volumetric lock-up (Budiansky & Fleck 1993) on the compressive strength is also explored.

2. Problem formulation and finite element implementation

The fibre composite is treated as a smeared-out anisotropic Cosserat continuum, with a bending resistance set by the fibre diameter d. Macroscopic stress and strain quantities are used for the smeared-out homogeneous composite. The governing field equations and constitutive law for the fibre composite is implemented via a finite element code, using six noded triangular elements with three degrees of freedom at each node (two displacements and one rotation). The finite element procedure is based upon an incremental Lagrangian formulation of the general finite deformation of the composite and can deal with both geometrical and material nonlinearities. A version of the modified Riks algorithm (Crisfield 1991) is adopted to handle the snap-back behaviour associated with the microbuckling response. An imperfection in the form of fibre waviness is included in the formulation.

(*a*) *Kinematics and definition of stresses*

The undeformed and deformed configurations are shown in figure 1*a*. Cartesian base vectors $(\boldsymbol{e}_1, \boldsymbol{e}_2)$ are introduced within the plane of deformation and are oriented such that the $\boldsymbol{e}_1$ direction is taken to be parallel to the fibre direction of the fully aligned unidirectional composite in the initial configuration. A material point is identified by the position vector $\boldsymbol{x}$ in the initial undeformed configuration and undergoes a finite in-plane displacement $\boldsymbol{u}$ to a position $\boldsymbol{X}$ in the current, deformed configuration as shown in figure 1*a*. A material point is also subjected to an independent micro rotation θ_f about the out-of-plane $\boldsymbol{e}_3$-axis. We assume that the fibres have an initial misalignment in the form of a rotation $\bar{\phi}(\boldsymbol{x})$ about the $\boldsymbol{e}_3$-axis, and upon deformation the fibres rotate through an additional angle $\phi(\boldsymbol{x})$ about the $\boldsymbol{e}_3$-axis to a total misalignment of $\phi_t = \bar{\phi} + \phi$. It is convenient to introduce an orthogonal curvilinear coordinate system (ξ_1, ξ_2) in the deformed configuration and to align the ξ_1 direction with the deformed fibre direction (see figure 1*a*). The physical distance along the ξ_1 direction is denoted by s_1 and the physical distance along the ξ_2 direction is denoted by s_2. The curvilinear coordinate system (ξ_1, ξ_2) is fully specified upon selecting arbitrarily a fibre as the base curve $\xi_2 = 0$, along which $\xi_1 = s_1$, and an orthogonal base

curve along which $\xi_2 = s_2$. In our development, tensors such as stress and strain will be expressed in terms of their physical components with respect to the ortho-normal unit base vectors $(\boldsymbol{\varepsilon}_1, \boldsymbol{\varepsilon}_2)$; spatial gradients in the deformed configuration will also be expressed in terms of the physical distances s_1 and s_2.

Consider a representative material element in the deformed configuration (see figure 1*b*). The element is subjected to a longitudinal compressive stress component σ_{L} aligned with the fibre direction, a sliding shear stress τ_{S}, a transverse shear stress τ_{T} and a transverse tensile stress σ_{T}. The fibres embedded in the material offer bending resistance; thus the representative material element carries a bending moment per unit area, or couple stress, m. The above stress measures are taken as Cauchy stress components in the current configuration; they are related most naturally to the orthogonal curvilinear coordinate system (ξ_1, ξ_2). On writing the Cauchy stress $\boldsymbol{\sigma} = \sigma_{ij}\boldsymbol{\varepsilon}_i\boldsymbol{\varepsilon}_j$ in terms of the stress quantities defined above we have

$$\sigma_{11} = \sigma_{\mathrm{L}}, \quad \sigma_{22} = \sigma_{\mathrm{T}}, \quad \sigma_{21} = \tau_{\mathrm{S}} \quad \text{and} \quad \sigma_{12} = \tau_{\mathrm{T}}. \tag{2.1}$$

We assume that the composite suffers a large deformation associated with large fibre rotation, large shear and transverse strains and small normal strain parallel to the local fibre direction. The strain rate is defined with respect to the current, deformed configuration. The strain rate can be expressed straightforwardly in terms of the orthogonal curvilinear coordinate system (ξ_1, ξ_2), as shown in figure 1*a*. The fundamental kinematic variables in the problem are the velocity $\boldsymbol{v}(\boldsymbol{X})$ and the rate of rotation of the fibre cross-section $\dot{\theta}_{\mathrm{f}}(\boldsymbol{X})$: this is analogous to Timoshenko beam theory and to Mindlin plate theory. The velocity gradient $\boldsymbol{D}$ is simply $\boldsymbol{D} = \nabla \boldsymbol{v}$ and the curvature rate is $\dot{\kappa} \equiv \partial \dot{\theta}_{\mathrm{f}}/\partial s_1$. Then, following Fleck & Shu (1995), the internal virtual work rate per unit current volume is written in the form of general Cosserat theory as

$$\dot{W} = \sigma_{11}D_{11} + \sigma_{22}D_{22} + \sigma_{12}(D_{12} - \dot{\theta}_{\mathrm{f}}) + \sigma_{21}(D_{21} + \dot{\theta}_{\mathrm{f}}) + m\dot{\kappa}. \tag{2.2}$$

Now introduce the extensional strain rate $\dot{e}_{\mathrm{L}} = D_{11}$, the transverse strain rate $\dot{e}_{\mathrm{T}} = D_{22}$ and the sliding shear rate $\dot{\gamma}_{\mathrm{S}}$ defined by

$$\dot{\gamma}_{\mathrm{S}} \equiv D_{12} + D_{21}. \tag{2.3}$$

The rate of fibre rotation is given by $\dot{\phi}_{\mathrm{t}} = D_{12}$. Note that the total strain quantities are simply given by integrating the strain rates over the deformation history. The internal work rate (2.2) can be re-expressed as

$$\dot{W} = \sigma_{\mathrm{L}}\dot{e}_{\mathrm{L}} + \sigma_{\mathrm{T}}\dot{e}_{\mathrm{T}} + \tau_{\mathrm{S}}\dot{\gamma}_{\mathrm{S}} + (\tau_{\mathrm{S}} - \tau_{\mathrm{T}})(\dot{\theta}_{\mathrm{f}} - D_{12}) + m\dot{\kappa}. \tag{2.4}$$

(*b*) *The deformation theory solid*

It remains to stipulate a constitutive law to relate stress rates to strain rates. Budiansky & Fleck (1993) proposed the following deformation theory constitutive law governing the transverse stress σ_{T} and shear stress τ_{S} of

$$\gamma_{\mathrm{S}} = \frac{\tau_{\mathrm{S}}}{G_{\mathrm{S}}(\tau_{\mathrm{e}})}, \quad e_{\mathrm{T}} = \frac{\sigma_{\mathrm{T}}}{R^2 G_{\mathrm{S}}(\tau_{\mathrm{e}})}. \tag{2.5}$$

Here, $R^2 = E_{\mathrm{T}}/G$ where E_{T} is the transverse Young's modulus and G is the in-plane longitudinal shear modulus of the composite. The effective stress τ_{e} and effective strain γ_{e} are defined as

$$\tau_{\mathrm{e}} = \sqrt{\tau_{\mathrm{S}}^2 + \sigma_{\mathrm{T}}^2/R^2}, \quad \gamma_{\mathrm{e}} = \sqrt{\gamma_{\mathrm{S}}^2 + R^2 e_{\mathrm{T}}^2}, \tag{2.6}$$

respectively, and are related through the simple shear constitutive law of

$$\gamma_{\mathrm{e}} = \frac{\tau_{\mathrm{e}}}{G_{\mathrm{S}}(\tau_{\mathrm{e}})}. \tag{2.7}$$

Specifically, a Ramberg–Osgood law is adopted:

$$\frac{\gamma_{\mathrm{e}}}{\gamma_{\mathrm{Y}}} = \frac{\tau_{\mathrm{e}}}{\tau_{\mathrm{Y}}} + \frac{3}{7}\left(\frac{\tau_{\mathrm{e}}}{\tau_{\mathrm{Y}}}\right)^{n}, \tag{2.8}$$

where $(\tau_{\mathrm{Y}}, \gamma_{\mathrm{Y}}, n)$ are taken to be material constants. The shear yield stress τ_{Y} and shear yield strain γ_{Y} are related via $\tau_{\mathrm{Y}} = G\gamma_{\mathrm{Y}}$. This gives a secant modulus $G_{\mathrm{S}} \equiv \tau_{\mathrm{e}}/\gamma_{\mathrm{e}}$ of

$$G_{\mathrm{S}}(\tau_{\mathrm{e}}) = G \Big/ \left(1 + \frac{3}{7}\left(\frac{\tau_{\mathrm{e}}}{\tau_{\mathrm{Y}}}\right)^{n-1}\right). \tag{2.9}$$

It is convenient to express the constitutive law in an incremental form for implementation within the large deformation framework. We write (2.5) in the rate form

$$\dot{\tau}_{\mathrm{S}} = G_{\mathrm{S}}\dot{\gamma}_{\mathrm{S}} + G'_{\mathrm{S}}\dot{\tau}_{\mathrm{e}}\gamma_{\mathrm{S}}, \quad \dot{\sigma}_{\mathrm{T}} = R^2 G_{\mathrm{S}}\dot{e}_{\mathrm{T}} + R^2 G'_{\mathrm{S}}\dot{\tau}_{\mathrm{e}} e_{\mathrm{T}} \tag{2.10}$$

and substitute into the rate form of the first equation of (2.6),

$$\tau_{\mathrm{e}}\dot{\tau}_{\mathrm{e}} = \tau_{\mathrm{S}}\dot{\tau}_{\mathrm{S}} + \sigma_{\mathrm{T}}\dot{\sigma}_{\mathrm{T}}/R^2, \tag{2.11}$$

to get

$$\dot{\tau}_{\mathrm{e}} = \frac{G_{\mathrm{S}}^2}{G_{\mathrm{S}} - \tau_{\mathrm{e}}G'_{\mathrm{S}}}\left(\frac{\tau_{\mathrm{S}}}{\tau_{\mathrm{e}}}\dot{\gamma}_{\mathrm{S}} + \frac{\sigma_{\mathrm{T}}}{\tau_{\mathrm{e}}}\dot{e}_{\mathrm{T}}\right). \tag{2.12}$$

Here $G'_{\mathrm{S}} \equiv \mathrm{d}G_{\mathrm{S}}/\mathrm{d}\tau_{\mathrm{e}}$. By substituting (2.12) into (2.10), we arrive at the constitutive relations in rate form

$$\dot{\tau}_{\mathrm{S}} = G_{\mathrm{S}}\dot{\gamma}_{\mathrm{S}} + \frac{\tau_{\mathrm{e}}G'_{\mathrm{S}}G_{\mathrm{S}}}{G_{\mathrm{S}} - \tau_{\mathrm{e}}G'_{\mathrm{S}}}\frac{\tau_{\mathrm{S}}}{\tau_{\mathrm{e}}}\left(\frac{\tau_{\mathrm{S}}}{\tau_{\mathrm{e}}}\dot{\gamma}_{\mathrm{S}} + \frac{\sigma_{\mathrm{T}}}{\tau_{\mathrm{e}}}\dot{e}_{\mathrm{T}}\right), \tag{2.13a}$$

$$\dot{\sigma}_{\mathrm{T}} = R^2 G_{\mathrm{S}}\dot{e}_{\mathrm{T}} + \frac{\tau_{\mathrm{e}}G'_{\mathrm{S}}G_{\mathrm{S}}}{G_{\mathrm{S}} - \tau_{\mathrm{e}}G'_{\mathrm{S}}}\frac{\sigma_{\mathrm{T}}}{\tau_{\mathrm{e}}}\left(\frac{\tau_{\mathrm{S}}}{\tau_{\mathrm{e}}}\dot{\gamma}_{\mathrm{S}} + \frac{\sigma_{\mathrm{T}}}{\tau_{\mathrm{e}}}\dot{e}_{\mathrm{T}}\right). \tag{2.13b}$$

It remains to stipulate constitutive relations for the longitudinal stress rate $\dot{\sigma}_{\mathrm{L}} = \dot{\sigma}_{11}$, the transverse shear stress rate $\dot{\tau}_{\mathrm{T}}$ and the couple stress rate $\dot{m}$. We follow Fleck & Shu (1995) and assume that $\dot{\tau}_{\mathrm{T}}$ is given by

$$\dot{\tau}_{\mathrm{T}} = cG_{\mathrm{f}}(D_{12} - \dot{\theta}_{\mathrm{f}}) + (1-c)\dot{\tau}_{\mathrm{S}}, \tag{2.14}$$

where c is the fibre volume fraction and G_{f} is the longitudinal shear modulus of the fibres. The couple stress rate is related to the micro curvature rate through

$$\dot{m} = \tfrac{1}{16}E_{\mathrm{L}}d^2\dot{\kappa} \tag{2.15}$$

and the longitudinal stress in the composite $\dot{\sigma}_{\mathrm{L}}$ is given by

$$\dot{\sigma}_{\mathrm{L}} = E_{\mathrm{L}}\dot{e}_{\mathrm{L}}, \tag{2.16}$$

where E_{L} is the longitudinal modulus of the composite.

The finite element program has already been described in detail by Fleck & Shu (1995) and a user manual has been produced (Shu & Fleck 1995). The code is implicit and Lagrangian in nature and relies upon the principle of virtual work in rate form. Details of the formulation for the general case of in-plane multiaxial loading are given in Appendix A.

(i) *The role of volumetric lock-up*

It is commonly observed that the fibres rotate within a microbuckle band until the transverse strain within the band vanishes: at this point volumetric *lock-up* of the matrix occurs and further rotation of the fibres within the band is prevented (Budiansky & Fleck 1993). It is thought that the matrix can dilate by voiding but is unable to accommodate compressive hydrostatic strains exceeding elastic magnitude. Two versions of the finite element model are employed in the current study.

(1) *Volumetric lock-up is neglected.* It is assumed that compressive hydrostatic strains can develop in microbuckled material and that the above combined constitutive law remains valid for compressive transverse strains.

(2) *Volumetric lock-up is included.* We assume that lock-up occurs when the total transverse strain e_T approaches zero from a state of positive transverse strain. Thereafter, the effective stress and effective strain for the deformation theory solid are taken as

$$\tau_e = |\tau_S|, \quad \gamma_e = |\gamma_S|, \quad \text{for } \sigma_T < 0 \tag{2.17}$$

and the transverse compressive response is given by

$$\sigma_T = E_T e_T, \quad \text{for } \sigma_T < 0. \tag{2.18}$$

The rate form of the constitutive law governing τ_S and σ_T after lock-up is

$$\dot{\tau}_S = \frac{G_S^2}{G_S - \tau_e G_S'}\dot{\gamma}_S \quad \text{and} \quad \dot{\sigma}_T = E_T \dot{e}_T. \tag{2.19}$$

Most of the results detailed below neglect lock-up. However, exploratory calculations were performed to explore the significance of volumetric lock-up. In general, it was found that lock-up has a negligible effect on compressive strength: when lock-up occurs, the compressive strength is increased by less than a few percent. Specific details are given in §§ 3 and 4.

(ii) *Specification of the composite properties*

In all calculations contained in this paper, the following material constants are assumed unless stated otherwise: $E_L/\tau_Y = 4 \times 10^3$, $E_T/\tau_Y = 4 \times 10^2$, $G/\tau_Y = 10^2$, $n = 3$ and $c = 0.6$. The fibre longitudinal shear modulus G_f is assigned a value of 4×10^2. The above parameters imply that $R = 2$ and the shear yield strain $\gamma_Y = 1\%$. The above values are representative of those for carbon fibre reinforced epoxy composites.

(*c*) *Infinite band of imperfection*

Consider a system with an infinitely long microbuckle band inclined at an angle β from the transverse direction (see figure 2*a*). Following Fleck & Shu (1995), the distribution of initial fibre misalignment $\bar{\phi}$ is taken to be

$$\bar{\phi} = \bar{\phi}_0 \cos \tfrac{1}{2}\pi\rho, \quad \text{for } \rho < 1, \tag{2.20}$$

where $\rho = 2x'/w$ and $x' = x\cos\beta + y\sin\beta$. Elsewhere the fibre misalignment $\bar{\phi}$ is taken to vanish. Here, β is the initial orientation angle of the microbuckle band relative to the transverse direction of the fibre composite and w is the initial band width. For all computations in this paper, a typical misalignment of $\bar{\phi}_0/\gamma_Y = 4$ is assumed. Recall that $\gamma_Y = 1\%$, giving $\bar{\phi}_0 \approx 2.3°$.

The focus of this paper is to predict the compressive initiation strength σ_c of a

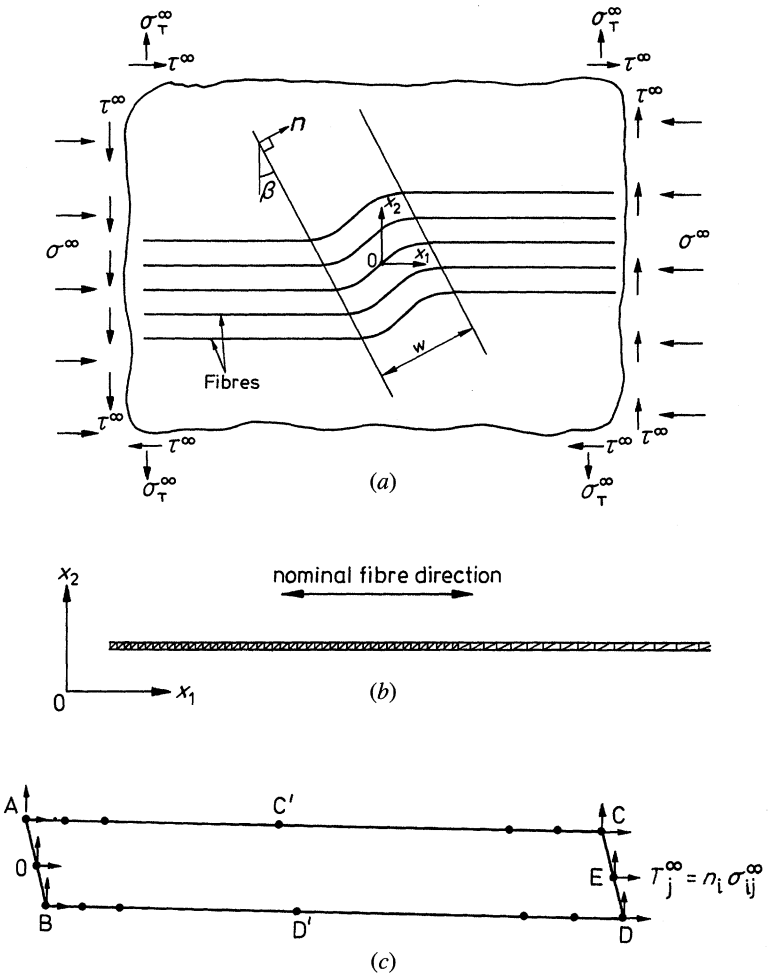

Figure 2. (*a*) Geometry of an infinitely long microbuckle band under remote multiaxial loading. (*b*) The mesh for analysing an infinitely long microbuckle band of $\beta = 0°$; the mesh has 200 elements and 603 nodes. (*c*) The geometry and boundary conditions for an infinite band analysis.

fibre composite under remote multiaxial loading, i.e. $\sigma_{22}^{\infty} = \sigma_{\mathrm{T}}^{\infty}$ and $\tau_{12}^{\infty} = \tau_{21}^{\infty} = \tau^{\infty}$. The remote couple stress m^{∞} vanishes. For simplicity, we assume that the loading is applied in a two-stage piecewise proportional manner, as follows. First, the remote transverse stress and shear stress are increased in fixed proportion from zero to a desired level. During this stage, no remote axial compression stress σ_{11}^{∞} is applied. Second, while holding the remote transverse stress and shear stress fixed, a compressive stress of $\sigma_{11}^{\infty} = -\sigma^{\infty}$ is applied. A pronounced snap-back response occurs after a maximum value σ_{c} of σ^{∞} has been attained; a modified Rik's algorithm is used in order to follow the unstable equilibrium path (Crisfield 1991).

Only half of the geometry needs to be analysed due to rotational symmetry of the problem about any arbitrary midpoint of the band. The correlation of fibre misalignment along the band direction allows us to analyse the problem with a simple mesh of width $1d$ and length $400d$. A typical mesh for an infinite band analysis, containing 200 elements and 603 nodes, with a total of 1809 degrees of freedom, is shown in figure 2*b*. The boundary conditions are specified in Appendix B.

(d) *Elliptical region of imperfection*

In general, a microbuckle originates and grows in a crack-like manner from an initial defect, often in the form of a localized patch of fibre waviness. Following Fleck & Shu (1995), we assume that the initial fibre misalignment angle $\bar{\phi}$ is confined to an ellipse of length ℓ, width w and inclination β, as defined in figure 3*a*. The distribution of $\bar{\phi}$ within the ellipse is taken as

$$\bar{\phi} = \bar{\phi}_0 \cos \tfrac{1}{2}\pi\rho, \quad \rho < 1, \tag{2.21}$$

where ρ is defined by

$$\rho = \{(2x'/w)^2 + (2y'/\ell)^2\}^{1/2} \tag{2.22}$$

in terms of the rotated coordinate frame

$$x' = x\cos\beta + y\sin\beta \quad \text{and} \quad y' = -x\sin\beta + y\cos\beta. \tag{2.23}$$

The maximum value of fibre misalignment is taken as $\bar{\phi}_0/\gamma_Y = 4$ and the fibre misalignment is assumed to vanish outside of the ellipse.

The composite is subjected to general in-plane multiaxial loading, as sketched in figure 3*a*. Consideration of rotational symmetry allows us to analyse only half of the specimen (see figure 3*b*). The left-hand boundary of the mesh is adjacent to the initial imperfection and is inclined at an angle β. Antisymmetric displacements are applied to this left-hand boundary, as shown in figure 3*b*. The remaining boundaries are subjected to uniform traction. A typical mesh for the finite imperfection case has been given previously by Fleck & Shu (1995).

3. Infinite band analysis

The simplest imperfection is in the form of an infinite band of fibre waviness, as sketched in figure 2*a*. It is instructive to determine the sensitivity of the compressive strength of an infinite band under multiaxial stressing to the following constitutive details: (i) the choice between deformation theory solid and flow theory solid; and (ii) the role of fibre bending resistance.

For an infinite band inclined at an angle β of more than a few degrees, the volumetric strain in the band is positive at maximum load and lock-up has no effect on compressive strength. Lock-up does occur for a band inclined at a sufficiently small value of β. Additional calculations were performed to determine the significance of lock-up for $\beta = 0°$. We found that the occurrence of lock-up increased the compressive strength by less than a few percent unless the band was wide ($w/d > 10$) and the loading involved a large component of remote shear ($\tau^\infty/\tau_Y = 0.5$). This exceptional case is discussed further in § 4 *c*. Results presented in the current section ignore the effects of volumetric lock-up.

(a) *Comparison between the predictions of deformation theory and flow theory*

To date, most analyses of plastic microbuckling have assumed the composite behaves as a deformation theory solid (see, for example, Slaughter *et al.* 1993; Fleck *et al.* 1995). Fleck & Shu (1995) adopted a flow theory version of the constitutive law for the composite. Experimental evidence suggests that a carbon fibre reinforced epoxy composite is neither an ideal deformation theory solid nor an ideal flow theory solid, but is rather a compromise between the two theories (Jelf & Fleck 1995). It is instructive to compare the predicted compressive strengths for the two theories.

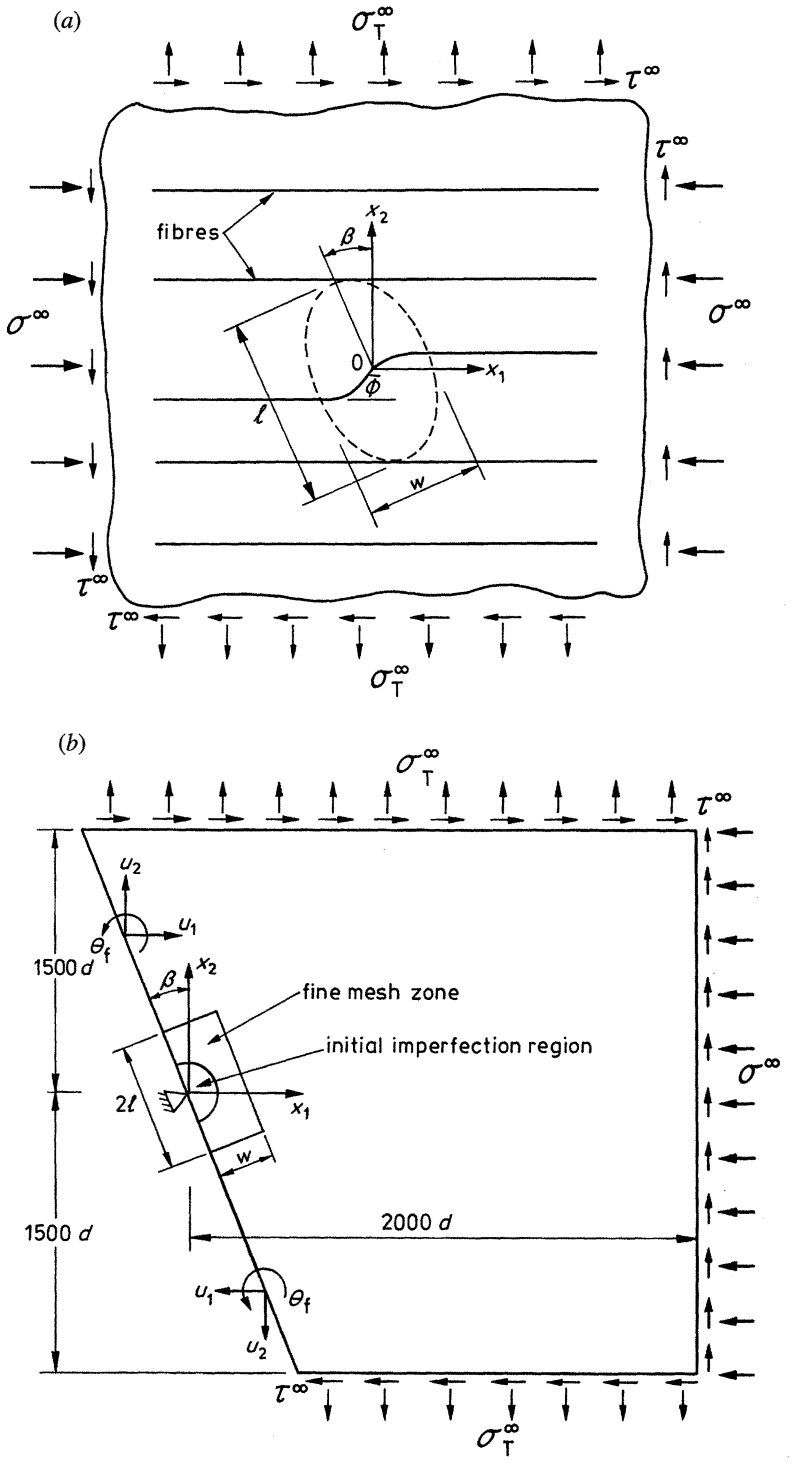

Figure 3. (*a*) Sketch of a fibre composite under remote multiaxial loading with an ellipse of initial fibre waviness. The lengths of the two major axes of the ellipse are ℓ and w. (*b*) Sketch of the geometry and boundary conditions for analysis of the finite imperfection.

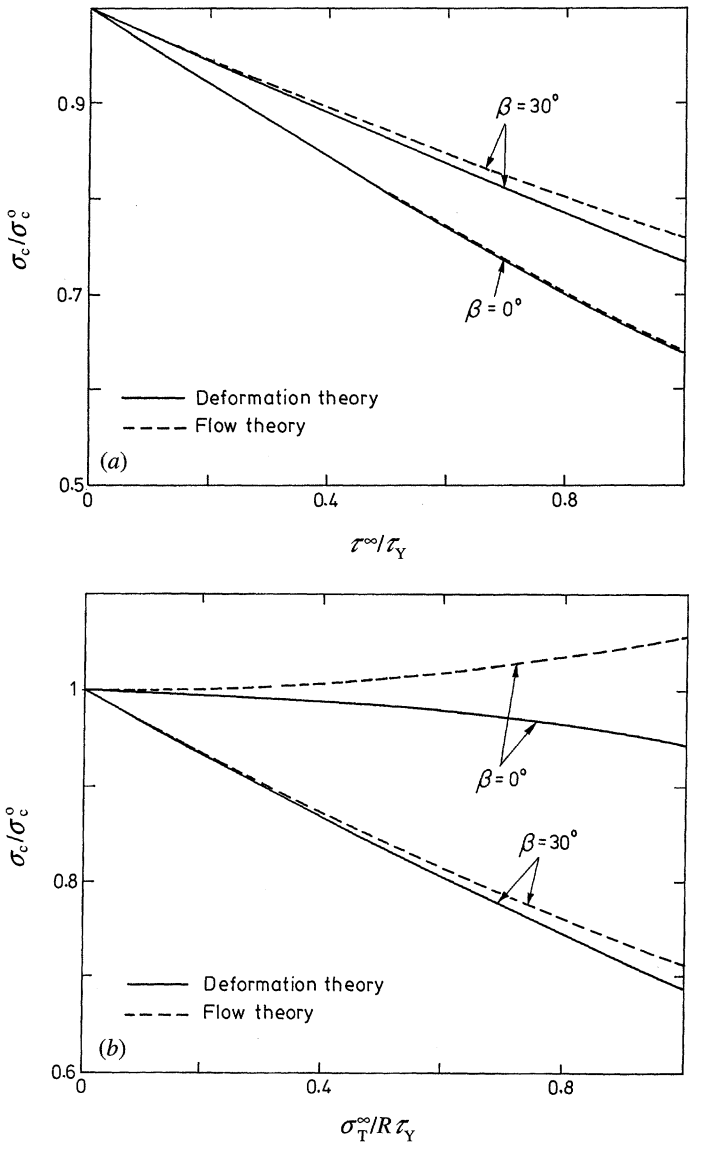

Figure 4. Comparison between the predictions of deformation theory and flow theory for an infinite band of initial waviness, with $w = 20d$, $\bar{\phi}_0/\gamma_Y = 4$ and $n = 3$. (*a*) Knock-down factor due to remote shear. (*b*) Knock-down factor due to remote transverse tension.

We address this problem by studying the response of an infinite band with an initial width of $w = 20d$ (recall that d is the fibre diameter) and initial fibre misalignment angle $\bar{\phi}_0/\gamma_Y = 4$.

The maximum compressive stress σ_c is calculated for a range of remote multiaxial loading. Preliminary finite element calculations reveal that the uniaxial compressive strength σ_c^0 differs by less than 0.1% for the two theories. The *knock-down* factor for the compressive strength, σ_c/σ_c^0, is plotted in figure 4*a* for the case of remote shear and in figure 4*b* for the case of remote transverse tension. In all cases the difference is less than 10%. The predictions for deformation theory and flow theory are

Table 1. *Value of* c_1 *for* $R = 2$

β (deg)	$n = 3$	$n = 5$	$n = 10$	$n = 100$	$1/\alpha$
0	0.408	0.590	0.723	0.767	1.0
5	0.407	0.588	0.716	0.769	0.985
10	0.405	0.567	0.705	0.748	0.943
15	0.387	0.543	0.662	0.716	0.881
20	0.354	0.513	0.615	0.681	0.808
25	0.328	0.469	0.565	0.636	0.731
30	0.283	0.425	0.520	0.589	0.655

Table 2. *Value of* c_2 *for* $R = 2$

β (deg)	$n = 3$	$n = 5$	$n = 10$	$n = 100$	$\tan\beta/\alpha$
0	0	0	0	0	0
5	0.098	0.141	0.150	0.179	0.086
10	0.182	0.228	0.303	0.298	0.166
15	0.231	0.318	0.385	0.410	0.236
20	0.277	0.396	0.467	0.508	0.294
25	0.319	0.453	0.537	0.587	0.341
30	0.336	0.498	0.605	0.657	0.378

in closer agreement when the remote loading is predominantly shear than when it is transverse tension. Also, the agreement is generally better for an inclined band than for a transverse band ($\beta = 0$). Since it is commonly observed that a microbuckle band is inclined at an angle, typically 10–30°, from the transverse direction, we conclude that the deformation and flow theories give similar predictions of compressive strength. Henceforth, we shall assume the composite is a deformation theory solid in the presentation of results.

(*b*) *Comparison between kinking analysis and bending analysis*

Slaughter *et al.* (1993) predicted the compressive strength under remote multiaxial loading by carrying out a so-called *kinking* analysis, i.e. neglecting the bending stiffness of the fibres. Here we use our finite element code, which assumes a finite fibre bending stiffness, to predict the compressive strengths under remote multiaxial loading. In all cases we assume the initial fibre waviness is specified by (2.20), with $w = 20d$ and $\bar{\phi}_0/\gamma_Y = 4$. For the case of a band inclined at $\beta = 30°$, the knock-down in compressive strength is shown in figure 5*a* for shear loading and in figure 5*b* for transverse tension. Parallel results are given in figures 6*a*,*b* for a transverse band ($\beta = 0°$). We conclude from figures 5 and 6 that the effect of fibre bending resistance on the knock-down response is small. A similar conclusion was drawn by Fleck *et al.* (1995) for the case of uniaxial compression.

The knock-down in compressive strength due to the presence of in-plane shear stress and transverse stress is summarized in the form of contour plots, as shown in

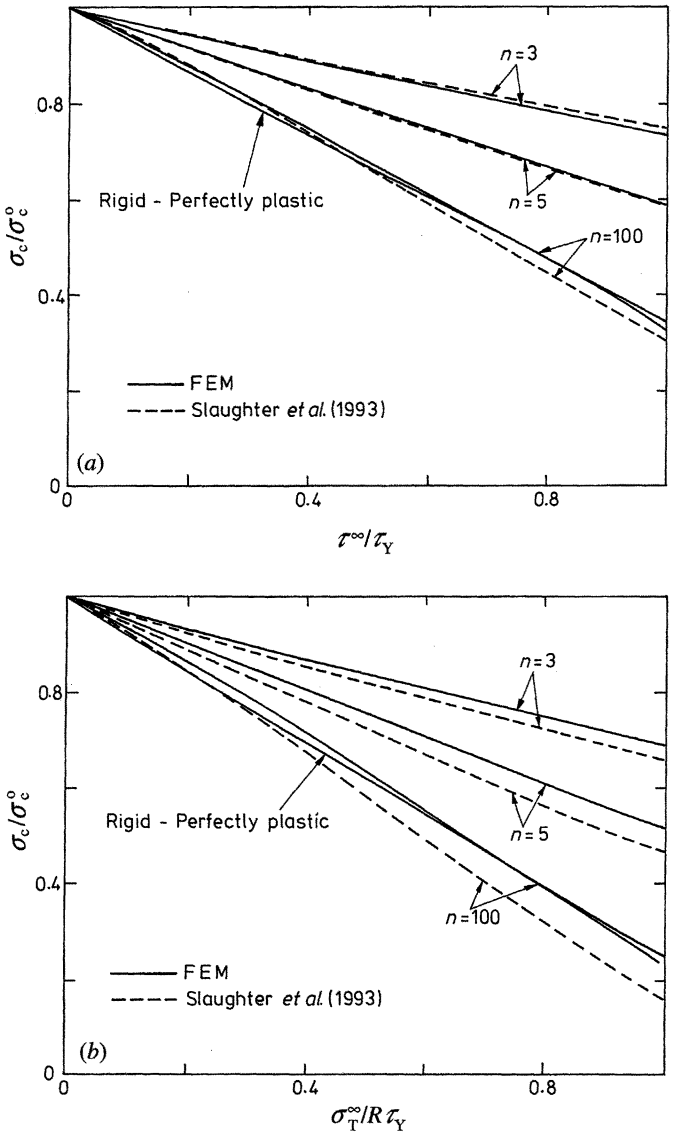

Figure 5. Comparison between the predictions of kinking theory and couple stress theory for an inclined infinite band of initial waviness, with $\beta = 30°$, $w = 20d$, $\bar{\phi}/\gamma_Y = 4$ and $n = 3$. (*a*) Knock-down factor due to remote shear. (*b*) Knock-down factor due to remote transverse tension.

figure 7. Results are displayed for $n = 3$ and $\bar{\phi}_0/\gamma_Y = 4$, and for two values of band inclination, $\beta = 0°$ and $\beta = 30°$. We limit results to the practical range of $\tau_e^\infty \equiv \sqrt{(\tau^\infty)^2 + (\sigma_T^\infty/R)^2} \leqslant \tau_Y$. It is noted that contour lines of constant knock-down factor are remarkably straight for the inclined band ($\beta = 30°$) and are reasonably straight in most of the domain for the transverse band ($\beta = 0°$). Thus, the data are well approximated by a linear relation of the form

$$\frac{\sigma_c}{\sigma_c^0} = 1 - c_1\frac{\tau^\infty}{\tau_Y} - c_2\frac{\sigma_T^\infty}{R\tau_Y}, \tag{3.1}$$

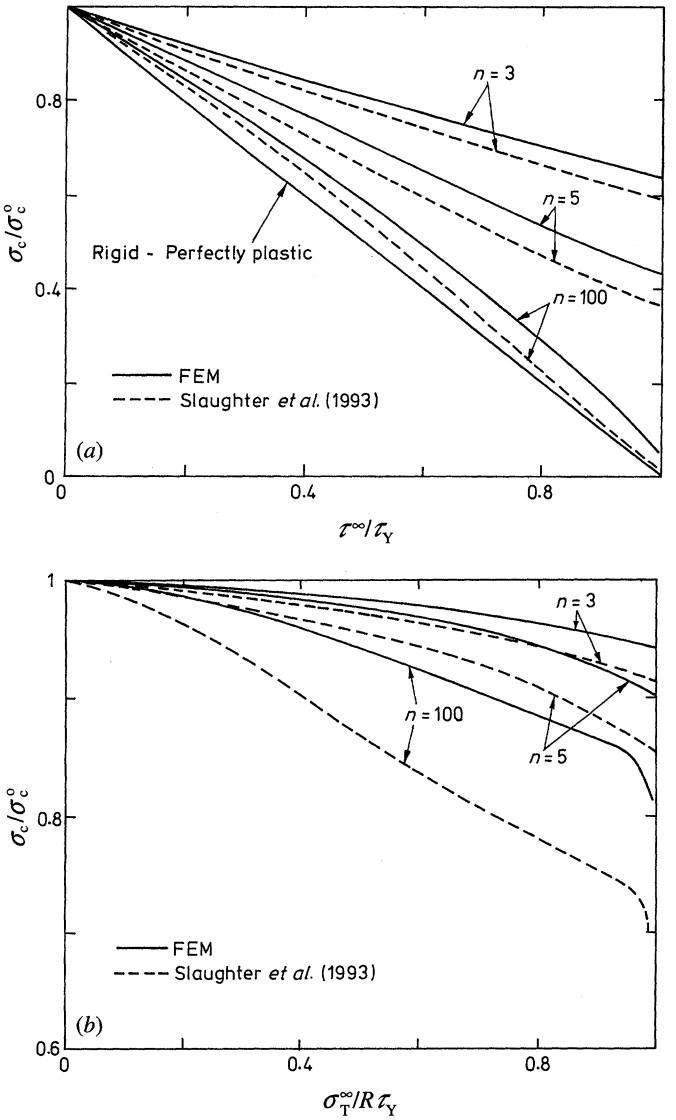

Figure 6. Comparison between the predictions of kinking theory and couple stress theory for a transverse infinite band of initial waviness, with $\beta = 0°$, $w = 20d$, $\bar{\phi}_0/\gamma_Y = 4$ and $n = 3$. (*a*) Knock-down factor due to remote shear. (*b*) Knock-down factor due to remote transverse tension.

where the parameters c_1 and c_2 depend upon the particular values of β and n, as detailed below. (A parametric study indicated that the dependence upon R and on initial width of band is slight.) Relation (3.1) is a generalization of the formula derived for a rigid perfectly plastic solid by Slaughter *et al.* (1993)

$$\frac{\sigma_c}{\sigma_c^0} = 1 - \frac{\tau^\infty}{\alpha\tau_Y} - \frac{\sigma_T^\infty}{\alpha\tau_Y}\tan\beta, \tag{3.2}$$

where $\alpha = \sqrt{1 + R^2\tan^2\beta}$. Values for c_1 and c_2 are given in tables 1 and 2, respectively, for $R = 2$. The last column in tables 1 and 2 is the coefficient for the rigid perfectly plastic solid given by (3.2). The rigid perfectly plastic results gives an

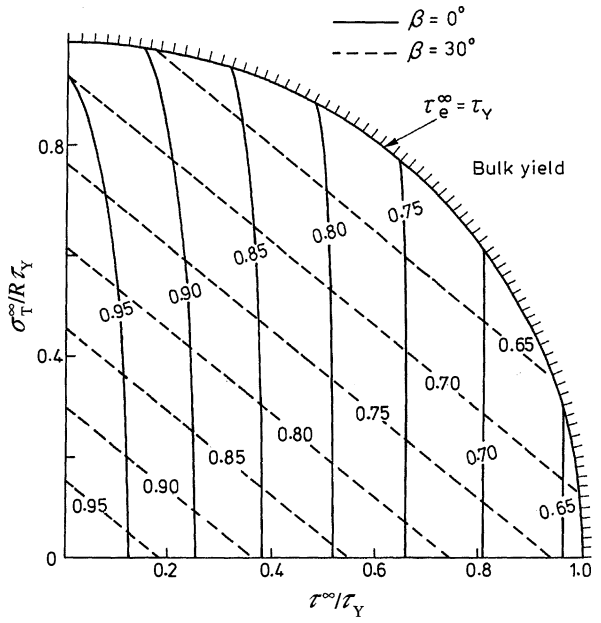

Figure 7. Contour plot of the knock-down factor on the compressive strength for an infinite band of initial waviness under general multiaxial loading. $\beta = 0°$ and $30°$, $w = 20d$, $\bar{\phi}_0/\gamma_Y = 4$ and $n = 3$.

approximate guideline for the knock-down in compressive strength due to multiaxial stress.

We note from tables 1 and 2 (and from figures 5 and 6) that the knock-down factor σ_c/σ_c^0 for shear stress and transverse stress decreases with increasing n for all values of β considered. For any fixed value of n, the knock-down factor for shear stress increases with increasing β, whereas the knock-down factor for transverse tension decreases with increasing β.

4. Finite imperfection

Next, we assume that an initial imperfection exists in the form of fibre misalignment confined to an ellipse as described by equations (2.21)–(2.23) and shown in figure 3*a*. The effect of multiaxial loading on the compressive strength is explored for the elliptical imperfection in the following subsections. First, the compressive strength is given as a function of length and width of the ellipse. The role of the shape of the imperfection is addressed by comparing the behaviours for an ellipse, a circle and an infinite band. The effect upon the compressive strength of the physical size of the imperfection is then explored. Finally, the effect of multiaxial stress is summarized in the form of contour plots of the knock-down factor for compressive strength. Unless otherwise stated, the calculations reported ignore the effects of volumetric lock-up.

(*a*) *The effect of the aspect ratio of the elliptical imperfection upon multiaxial strength*

First, we consider an elliptical imperfection of fixed width $w = 20d$, oriented at an inclination $\beta = 0°$. The compressive strength is shown in figure 8 as a function

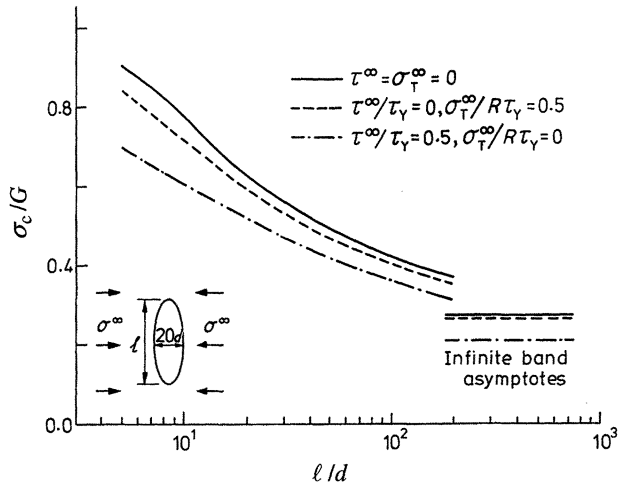

Figure 8. Compressive strength as a function of the length ℓ of an elliptical region of fibre misalignment under remote multiaxial loading. $\beta = 0°$, $w = 20d$, $\bar{\phi}_0/\gamma_Y = 4$ and $n = 3$.

of length ℓ, for a selection of values of τ^∞ and σ_T^∞, with $n = 3$ and $\bar{\phi}_0/\gamma_Y = 4$. The limit $\ell \to 0$ corresponds to the case of vanishing imperfection, while the limit $\ell \to \infty$ is the infinite band result. In the case of uniaxial compression at $\ell = 20d$, the compressive strength σ_c is midway between the Rosen elastic bifurcation value (for vanishing imperfection) and the infinite band result. At $\ell = 200d$, the compressive strength is only about 20% higher than that of an infinite band. Similar conclusions are drawn for the case of superposed remote shear and remote transverse tension. These findings imply that a relatively small region of fibre waviness leads to a serious reduction of the compressive strength. For example, the diameter of carbon fibres is of the order of 5 μm for commercial carbon fibre–epoxy composites. This implies that an imperfection of length 1–2 mm results in a compressive strength comparable to that of an infinite band.

The effect of the width w of an elliptical imperfection upon the compressive strength is given in figure 9, for a range of values of fixed length ℓ. Again, results are shown for a selection of multiaxial loading, and in all cases $\beta = 0$, $n = 3$ and $\bar{\phi}/\gamma_Y = 4$. It is clear from figure 9 that there is little effect of width of imperfection upon the compressive strength, for all values of w and ℓ considered. The dominant geometrical dimension in influencing compressive strength is the length ℓ of the band, as discussed above. Note that no calculations were performed for $w/d < 4$: we anticipate the compressive strength to increase sharply with diminishing w at $w/d < 4$. For example, in the case of uniaxial compression, the compressive strength attains the Rosen limit $\sigma_c = G$ as $w \to 0$.

(*b*) *The effects of the shape and size of the imperfection upon multiaxial strength*

The effects of the shape and size of the region of fibre waviness upon the uniaxial compressive strength are now addressed. Three geometries of initial imperfection are considered, as shown in the insert of figure 10 ((1) infinite band of width ℓ inclined at $\beta = 0°$; (2) circle of diameter ℓ; (3) ellipse of width $20d$ and length ℓ, oriented at $\beta = 0°$).

All three shapes of imperfection are described by (2.20)–(2.23), with $\bar{\phi}_0/\gamma_Y = 4$. The compressive strength as a function of imperfection size of each of the three shapes

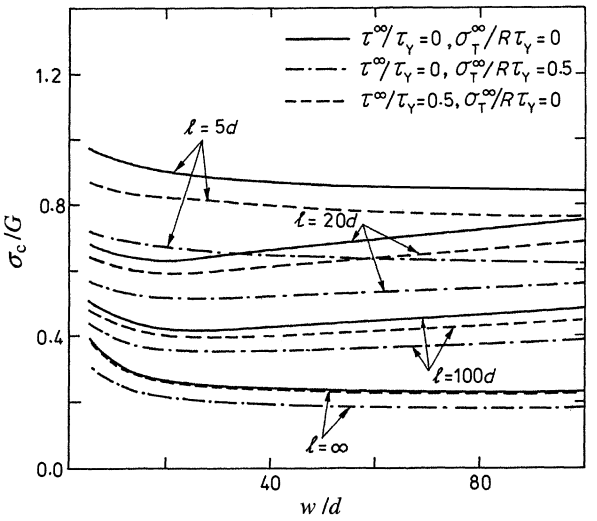

Figure 9. Compressive strength as a function of the width w of an elliptical region of fibre misalignment under remote multiaxial loading. $\beta = 0°$, $\bar{\phi}_0/\gamma_Y = 4$ and $n = 3$.

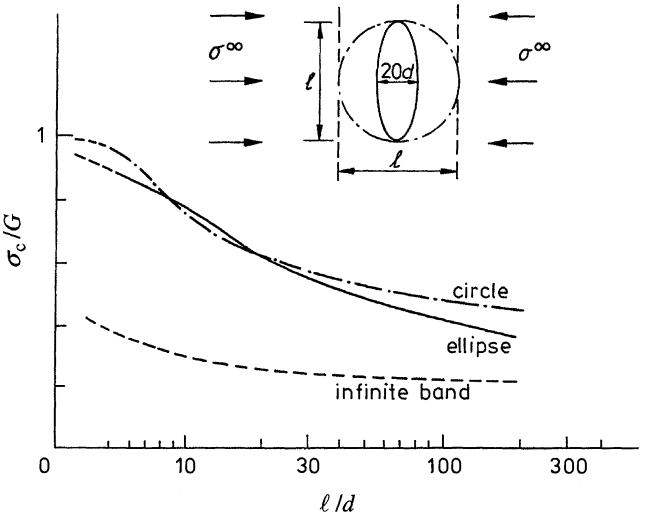

Figure 10. Effect of imperfection shape upon uniaxial compressive strength. $\beta = 0°$, $\bar{\phi}_0/\gamma_Y = 4$ and $n = 3$.

is shown in figure 10. We note that the infinite band prediction is significantly weaker than the other shapes for the ℓ/d values considered. In the limit of large ℓ/d (greater than about 30 for the infinite band and greater than about 300 for the circle and the ellipse), the strengths converge to the asymptote given by the kinking solution (58) of Budiansky & Fleck (1993). It is instructive to compare the strengths for the ellipse and for the circle at $\ell/d > 20$. Then, the circle circumscribes the ellipse; the circular patch has a larger physical size but gives less of a stress concentrating effect than the ellipse. These two factors compete, and result in the circle being slightly stronger than the ellipse, for the same value of ℓ/d. The main practical conclusion to draw from figure 10 is that compressive strength is significantly influenced by both the shape of the imperfection and by the size in relation to the fibre diameter d.

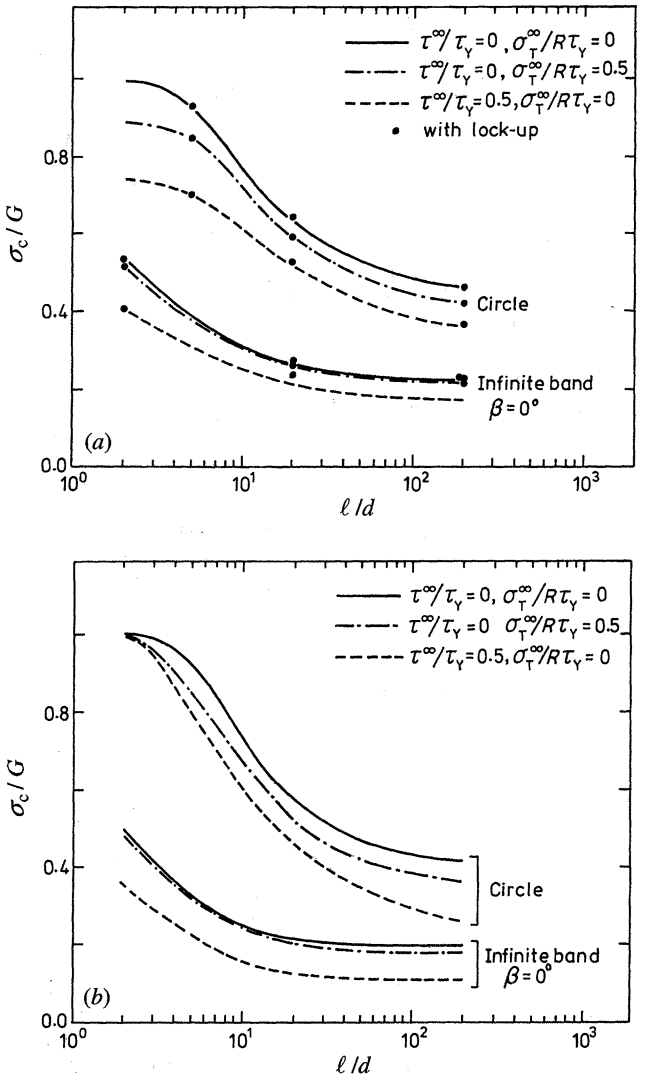

Figure 11. Effect of imperfection size upon compressive strength for multiaxial loading. Two shapes of imperfection region are considered: a circle of diameter ℓ and an infinite band of width ℓ at an inclination angle of $\beta = 0°$. For both geometries, $\bar{\phi}_0/\gamma_Y = 4$. The curves neglect the effect of lock-up and the discrete points (•) include the effect of lock-up. (*a*) $n = 3$ and (*b*) $n = 100$.

The effect of physical size of imperfection upon multiaxial strength is now considered. Attention is focused on a circular imperfection of diameter ℓ and an infinite band of width ℓ. The compressive strength for a selection of $(\tau^\infty, \sigma_T^\infty)$ values is given as a function of ℓ/d in figure 11*a* for $n = 3$ and in figure 11*b* for $n = 100$. A size effect is clearly demonstrated: as ℓ/d increases the compressive strength decreases to the kinking solution given by Slaughter *et al.* (1993).

(*c*) *The effect of fibre lock-up*

So far we have neglected the phenomenon of volumetric lock-up of fibre from our treatment. It is instructive to address the effects of lock-up upon the compressive

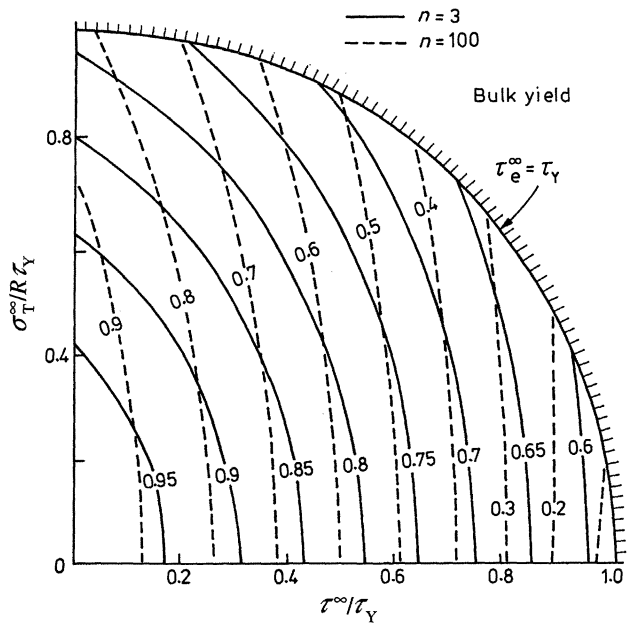

Figure 12. Contour plot of the knock-down factor for compressive strength, for a circular domain of fibre waviness under general multiaxial loading. The diameter of the circle is $20d$, $\bar{\phi}_0/\gamma_Y = 4$, $n = 3$ and 100.

strength under general multiaxial loading. Here, we examine the effect of lock-up on the compressive initiation strength for a circular imperfection and for an infinite band. For the case of an infinite band, from simple geometrical argument, it is known that the transverse strain within the microbuckle band vanishes and lock-up occurs at a rotation of $\phi = 2(\beta - \bar{\phi}_0)$ (Budiansky & Fleck 1993). For a band inclined at an angle β of more than a few degrees, lock-up is not yet attained at maximum load and thus the onset of lock-up does not affect the compressive strength. However, lock-up takes place immediately for the case of $\beta = 0°$. Here we choose $\beta = 0°$ for an infinite band analysis and present results in figure 11*a* for the case of lock-up neglected and lock-up included in the analysis. It is found that lock-up significantly increases the compressive strength of an infinite band only for the case of a wide band $\ell/d > 10$ and with a large value of superposed remote shear. In all other cases, lock-up has a negligible effect on compressive strength. Results on the effect of lock-up are included in figure 11*a* for a circular imperfection under multiaxial stressing. The effect of lock-up is insignificant.

(*d*) *Map of knock-down in strength for a finite imperfection under multiaxial loading*

Contours of the knock-down factor for the compressive strength due to in-plane shear and transverse tension for the case of a circular patch of waviness, of diameter $\ell = 20d$, are plotted in figure 12 for $n = 3$ and $n = 100$. We conclude from figure 12 that both shear stress and transverse stress significantly knock-down the compressive strength. The contours are approximately parallel but curved: there is a nonlinear coupling between the shear stress and transverse stress in knocking down the compressive strength. In the absence of transverse tension, the reduction in strength due to remote shear is fairly insensitive to the value of the strain hardening exponent and

to the precise geometry of the imperfection (compare figure 12 with the analogous map for the infinite band, figure 7). The knock-down due to transverse tension is sensitive to both the value of n and to the geometry.

5. Conclusions

The initiation of microbuckling of fibre composites under multiaxial loading has been investigated using a finite deformation finite element code based on the couple stress theory. As far as the initiation of microbuckling is concerned, deformation theory and flow theory constitutive laws give a negligible difference in compressive strength. Remote multiaxial stresses knock-down the compressive strength of an infinite band in an approximately linear fashion and an empirical formula is given to quantify the knock-down effect associated with the multiaxial stress. The initiation of microbuckling from a finite region of fibre misalignment has also been studied. The dominant geometric feature of the finite imperfection is its length in the transverse direction. An elliptical region of fibre waviness, of length exceeding $200d$, behaves as an infinite band. The phenomenon of fibre lock-up is incorporated in the finite element code and generally has little effect upon the initiation strength for both a finite imperfection and for an infinite band.

The authors thank Professor B. Budiansky and Dr M. P. F. Sutcliffe for many helpful discussions. Financial support from the ONR grant 0014-91-J-1916 is gratefully acknowledged. Additional support for J.Y.S. during the course of finishing the manuscript is provided by the US Department of Energy and Lawrence Livermore National Laboratory under contract no. W-7405-Eng-48.

Appendix A. Rate form of principle of virtual work

Fleck & Shu (1995) have derived the following rate form of the principle of virtual work:

$$\int_{\Omega_0} J\{(\dot{\sigma}_{ij} + \sigma_{ij}D_{kk} + \sigma_{kj}\varepsilon_{ki}\dot{\phi}_t + \sigma_{ik}\varepsilon_{kj}\dot{\phi}_t - \sigma_{kj}D_{ki})W_{ij} + (\dot{\sigma}_{ij} + \sigma_{ij}D_{kk})\varepsilon_{ji}\delta\theta_f + (\dot{m} + mD_{22})\delta\kappa_1\}\,\mathrm{d}\Omega_0 = \int_{S_0} (\dot{t}_j\delta u_j + \dot{q}\delta\theta_f)\,\mathrm{d}S_0. \quad (A\,1)$$

Here, ε_{ij} is the two-dimensional permutation symbol and $\boldsymbol{W}$ is the spatial gradient of the virtual displacement $\delta\boldsymbol{u}$, such that $\boldsymbol{W} = \nabla\delta\boldsymbol{u}$; J is the determinant of the deformation gradient tensor $\boldsymbol{F}$ and all components are physical components defined in an orthogonal curvilinear system co-rotating with the fibres. A subscript 0 denotes the undeformed configuration. Assume that an infinitesimal surface area vector $\mathrm{d}\boldsymbol{S}_0$ in the undeformed configuration is deformed into $\mathrm{d}\boldsymbol{S}$ in the current deformed configuration via $\boldsymbol{F}$. The nominal traction t_j $(j = 1, 2)$ and torque q per unit area of the undeformed surface are related to the true traction T_j and surface torque Q per unit area of the current deformed surface by

$$t_j\,\mathrm{d}S_0 = T_j\,\mathrm{d}S, \quad q\,\mathrm{d}S_0 = Q\,\mathrm{d}S. \quad (A\,2)$$

In a previous study, Fleck & Shu (1995) prescribed the loading in terms of t_j and q. Under uniaxial compression, the remote surface area does not deform, hence t_j equals T_j. Under multiaxial loading, the remote surface rotates and stretches; consequently,

the nominal and true tractions differ. In the current study the loading is prescribed in terms of the true traction components.

Now suppose a section, S_t, of the boundary is subjected to traction T_j $(j = 1, 2)$ and torque Q per unit surface area of the current deformed configuration given by

$$T_j = n_i(\sigma^0_{ij}(\boldsymbol{x}) + \lambda\Delta\sigma_{ij}(\boldsymbol{x})), \quad Q = n_1(m^0(\boldsymbol{x}) + \lambda\Delta m(\boldsymbol{x})), \tag{A 3}$$

where λ is a global loading parameter changing during the course of deformation. Here, n_i is the ith Cartesian component of the surface unit normal vector. The ith Cartesian component of the surface unit normal vector in the undeformed configuration is denoted as n^0_i. The nominal traction vector and the nominal couple stress traction follow from (A 2) and (A 3) as

$$\dot{t}_j\,\mathrm{d}S_0 = \mathrm{d}\dot{S}_i(\sigma^0_{ij} + \lambda\Delta\sigma_{ij}) + \dot{\lambda}\sigma_{ij}\,\mathrm{d}S_i, \quad \dot{q}\,\mathrm{d}S_0 = \mathrm{d}\dot{S}_1(m^0 + \lambda\Delta m) + \dot{\lambda}\Delta m\,\mathrm{d}S_1, \tag{A 4}$$

where $\mathrm{d}S_i = n_i\,\mathrm{d}S$. Now

$$\mathrm{d}\boldsymbol{S} = J\boldsymbol{F}^{-\mathrm{T}}\,\mathrm{d}\boldsymbol{S}_0, \tag{A 5}$$

where the superscript $-\mathrm{T}$ denotes the transpose of the inverse of the tensor, and so

$$\mathrm{d}\dot{\boldsymbol{S}} = (\dot{J}\boldsymbol{F}^{-\mathrm{T}} + J\dot{\boldsymbol{F}}^{-\mathrm{T}})\,\mathrm{d}\boldsymbol{S}_0. \tag{A 6}$$

On substituting $\dot{J} = JD_{kk}$ and $\dot{\boldsymbol{F}}^{-\mathrm{T}} = -\boldsymbol{D}\boldsymbol{F}^{-\mathrm{T}}$ into the above equation, we find that

$$\mathrm{d}\dot{\boldsymbol{S}} = J(D_{kk}\boldsymbol{F}^{-\mathrm{T}} - \boldsymbol{D}\boldsymbol{F}^{-\mathrm{T}})\,\mathrm{d}\boldsymbol{S}_0. \tag{A 7}$$

The rate form of the principle of virtual work follows from (A 1), (A 4) and (A 7) as

$$\begin{aligned}\int_{\Omega_0} J\{&(\dot{\sigma}_{ij} + \sigma_{ij}D_{kk} + \sigma_{kj}\varepsilon_{ki}\dot{\phi}_t + \sigma_{ik}\varepsilon_{kj}\dot{\phi}_t - \sigma_{kj}D_{ki})W_{ij} + (\dot{\sigma}_{ij} + \sigma_{ij}D_{kk})\varepsilon_{ji}\delta\theta_f \\ &+(\dot{m} + mD_{22})\delta\kappa_1\}\,\mathrm{d}\Omega_0 - \int_{S_0} J(F^{-1}_{ji}D_{kk} - F^{-1}_{jk}D_{ik})n^0_j(\sigma^0_{ik} + \lambda\Delta\sigma_{ik})\delta u_k\,\mathrm{d}S_0 \\ &- \int_{S_0} J(F^{-1}_{j1}D_{kk} - F^{-1}_{jk}D_{1k})n^0_j(m^0 + \lambda\Delta m)\delta\theta_f\,\mathrm{d}S_0 \\ &= \dot{\lambda}\int_{S_0} J(\Delta\sigma_{ij}F^{-1}_{ki}n^0_k\delta u_j + \Delta m F^{-1}_{k1}n^0_k\delta\theta_f)\,\mathrm{d}S_0.\end{aligned} \tag{A 8}$$

The above rate form is convenient when the remote Cauchy stress is a prescribed function of time. For example, (A 3) provides the appropriate boundary condition for an infinite band subjected to a prescribed remote stress.

Appendix B. Boundary conditions for infinite band analyses

Slaughter *et al.* (1993) have shown that under remote shear and transverse stresses, an infinitely long microbuckle band rotates slightly and the band angle changes during the deformation. After a finite deformation, any two material points which are initially aligned along the band direction remain aligned along the current band direction. Consider representative nodes C' and D' along the initial band direction, as shown in figure 2*c*. Their relative displacement equals the relative displacement of the two corner nodes C and D on the right-hand side of the mesh; also fibre rotations at C' and D' are identical. Thus,

$$u^{C'}_i - u^{D'}_i = u^C_i - u^D_i \quad \text{and} \quad \theta^{C'}_f = \theta^{D'}_f. \tag{B 1}$$

The nodal forces and nodal torques at these two nodes are related by

$$T_i^{C'} = -T_i^{D'} \quad \text{and} \quad Q^{C'} = -Q^{D'}. \tag{B 2}$$

For a particular node C' located one node along from the end node C, instead of enforcing its transverse nodal force to obey (B 2), the transverse displacement of the node C' is assumed to follow the constraint

$$u_2^{C'} = u_2^{C} \tag{B 3}$$

to remove the rigid body rotation of the composite. This ensures that remote fibres remain straight.

Now consider the boundary conditions on the two ends of the mesh. The nodal forces and nodal torques on nodes C, D and E at the right-hand boundary are prescribed in terms of the remote stress state, as laid down in Appendix A. To remove rigid body motion node O on the left-hand boundary is fixed ($u_1 = u_2 = 0$); the torque also vanishes at O. The relative displacements of nodes A and B are equated to those of C and D, and the fibre rotation at A is equated to that at B. Further, the sum of the nodal forces at A and B balance the sum of the nodal forces at C and D. Finally, the sum of the nodal torques on A and B vanishes.

References

Argon, A. S. 1972 *Fracture of composites. Treatise of materials sciences and technology*, vol. 1, pp. 79–114. New York: Academic.

Budiansky, B. 1983 Micromechanics. *Comput. Struct.* **16**, 3–12.

Budiansky, B. & Fleck, N. A. 1993 Compressive failure of fiber composites. *J. Mech. Phys. Solids* **41**, 183–211.

Budiansky, B. & Fleck, N. A. 1994 Compressive kinking of fibre composites: a topical review. *Appl. Mech. Rev.* **47**, S 246–250.

Crisfield, M. A. 1991 *Non-linear finite element analysis of solids and structures*, ch. 9, vol. 1. New York: John Wiley.

Fleck, N. A. & Jelf, P. M. 1995 Deformation and failure of a carbon fibre composite under combined shear and transverse loading. *Acta Metall. Mater.* **43**, 3001–3007.

Fleck, N. A. & Shu, J. Y. 1995 Microbuckle initiation in fibre composites: a finite element study. *J. Mech. Phys. Solids* **43**, 1887–1918.

Fleck, N. A., Deng, L. & Budiansky, B. 1995 Prediction of kink widths in compressed fiber composites. *J. Appl. Mech.* **62**, 329–337.

Rice, J. R. 1976 The localisation of plastic deformation. In *Theoretical and applied mechanics* (ed. W. T. Koiter), pp. 207–220. Amsterdam: North-Holland.

Rosen, B. W. 1965 Mechanics of composite strengthening: fibre composite materials. *Am. Soc. Metals Seminar* **3**, 37–75.

Shu, J. Y. & Fleck, N. A. 1995 User's manual for finite element code for microbuckling, Cambridge University Engineering Department, CUED/C-MATS/TR.224, May 1995.

Slaughter, W. S., Fleck, N. A. & Budiansky, B. 1993 Compressive failure of fibre composites: the roles of multiaxial loading and creep. *J. Appl. Mech.* **115**, 308–313.

Received 8 May 1996; revised 24 December 1996; accepted 14 February 1997